Electronic Supplementary Material (ESI) for ChemComm.
This journal is © The Royal Society of Chemistry 2020

Experimental Section

Synthesis of $MnMoO_4$/RGO

All the chemicals are of analytical grade and used as received. $MnMoO_4$/RGO was synthesized by a facile microwave-assisted hydrothermal method. In brief, 10 mg of GO was dispersed in 30 mL of deionized water under ultrasonic dispersion for 1 h, to which 0.1 mmol of $Na_2MoO_4 \cdot 2H_2O$ and 0.1 mmol of $Mn(CH_3COO)_2 \cdot 4H_2O$ were co-added under magnetic stirring to form a homogeneous solution. The mixture was sealed into a quartz vial, and treated by a microwave oven (2450 MHz) for 20 min. After cooling, the precipitates were separated by centrifugation, washed with ethanol and distilled water several times and then dried at 60°C for 12 h. The dried precipitates were placed into a horizontal quartz tube and heated to 800 °C for 3 h under Ar atmosphere to obtain $MnMoO_4$/RGO. For comparison, RGO were prepared by the same procedure without addition of $Na_2MoO_4 \cdot 2H_2O$ and $Mn(CH_3COO)_2 \cdot 4H_2O$.

Electrochemical experiments

The electrochemical measurements were carried out with an electrochemical workstation (CHI Instruments, Shanghai Chenhua Instrument Corp., China). A conventional three-electrode cell was employed with a carbon cloth (CC) sample as working electrode, an Ag/AgCl electrode as reference electrode, and a graphite rod as counter electrode. All potentials were referenced to reversible hydrogen electrode (RHE) by following equation: E_{RHE} (V)=$E_{Ag/AgCl}$+0.197+0.059×pH. The CC substrate was pretreated by soaking it in 0.5 M H_2SO_4 for 12 h, and then washed with deionized water several times and dried at 60 °C for 24 h. To prepare working electrode, 1 mg catalyst and 5 μL of Nafion (5 wt%) were ultrasonically dispersed in 100 μL of ethyl alcohol to form a homogeneous ink. Then 20 μL of catalyst ink was loaded on a 1×1 cm^2 CC substrate and dried under ambient condition. The NRR tests were performed using an H-type two-compartment electrochemical cell separated by a Nafion 211 membrane. The Nafion membrane was pretreated by boiling it in 5% H_2O_2 solution for 1 h, 0.5 M H_2SO_4 for 1 h and deionized water for 1 h in turn. During each

electrolysis, ultra-high-purity N_2 gas (99.999%) was continuously purged into the cathodic chamber at a flow rate of 20 mL min^{-1}. After each NRR electrolysis, the produced NH_3 and possible N_2H_4 were quantitatively determined by the indophenol blue method[2], and approach of Watt and Chrisp[3], respectively.

Determination of NH_3

4 mL of electrolyte was removed from the electrochemical reaction vessel. Then 50 μL of solution containing NaOH (0.75 M) and NaClO (ρ_{Cl} = ~4), 500 μL of solution containing 0.32 M NaOH, 0.4 M $C_7H_6O_3$, and 50 μL of $C_5FeN_6Na_2O$ solution (1 wt%) were respectively added into the electrolyte. After standing for 2 h, the UV-Vis absorption spectrum was measured and the concentration-absorbance curves were calibrated by the standard NH_4Cl solution with a series of concentrations.

$$\mathrm{NH_3\ yield}\ (\mu \mathrm{g\ h^{-1}\ mg_{cat.}^{-1}}) = \frac{c_{\mathrm{NH_3}} \times V}{t \times m} \quad (1)$$

Faradaic efficiency was calculated by the following equation:

$$\text{Faradaic efficiency}\ (\%) = \frac{3 \times F \times c_{\mathrm{NH_3}} \times V}{17 \times Q} \times 100\% \quad (2)$$

where c_{NH3} (μg mL^{-1}) is the measured NH_3 concentration, V (mL) is the volume of the electrolyte, t (h) is the reduction time and m (mg) is the mass loading of the catalyst on CC. F (96500 C mol^{-1}) is the Faraday constant, Q (C) is the quantity of applied electricity.

Determination of N_2H_4

5 mL of electrolyte was removed from the electrochemical reaction vessel. The 330 mL of color reagent containing 300 mL of ethyl alcohol, 5.99 g of $C_9H_{11}NO$ and 30 mL of HCl were prepared, and 5 mL of color reagent was added into the electrolyte. After stirring for 10 min, the UV-Vis absorption spectrum was measured and the concentration-absorbance curves were calibrated by the standard N_2H_4 solution with a series of concentrations.

Nuclear magnetic resonance measurement

^1H nuclear magnetic resonance (NMR) measurement was carried out using $^{15}N_2$ (99 % isotopic purity) as the feed gas. Prior to NMR measurement, $^{15}N_2$ was purified

by an acid trap (0.05 M H_2SO_4) to eliminate the NO_x and NH_3 contaminants [1]. The NRR experiment using $^{15}N_2$ was conducted at −0.40 V vs. RHE for 2 h. After NRR electrolysis, 4 mL of electrolyte was concentrated to ~1 mL and further acidized to pH ~2. The obtained electrolyte was mixed with 0.1 mL of deuterium oxide (D_2O) containing 100 ppm of dimethyl sulphoxide (DMSO) and 70 μL of D_2O for NMR spectroscopy measurement (500 MHz Bruker superconducting-magnet NMR spectrometer).

Characterizations

X-ray diffraction (XRD) pattern was recorded on a Rigaku D/max 2400 diffractometer. Transmission electron microscopy (TEM) and high-resolution transmission electron microscopy (HRTEM) were carried out on a Tecnai G^2 F20 microscope. X-ray photoelectron spectroscopy (XPS) analysis was conducted on a PHI 5702 spectrometer. The UV-vis absorbance measurements were performed on a MAPADA P5 spectrophotometer.

Calculation details

Spin-polarized DFT calculations were conducted using the plane-wave technique with exchange-correlation interactions modeled by the Perdew-Burke-Ernzerhof (PBE) generalized gradient approximation (GGA) functional, as implemented in the Cambridge sequential total energy package (CASTEP) [4]. DFT-D method was employed to calculate the van der Waals (vdW) interaction. The Brillouin zone was sampled with 3×3×1 k-points. The convergence of energy and forces were set to be 2×10^{-5} eV and 0.02 eV $Å^{-1}$, respectively. The kinetic cutoff energy for the plane wave basis was set at 450 eV. A 2 × 2 supercell with a vacuum layer of 15 Å was constructed, and then the $MnMoO_4$ (220) facet was cleaved to simulate the surface properties of $MnMoO_4$.

The Gibbs free energy (ΔG, 298 K) of reaction steps is calculated by [5]:

$$\Delta G=\Delta E+\Delta ZPE-T\Delta S \quad (3)$$

where ΔE is the adsorption energy, ΔZPE is the zero point energy difference and $T\Delta S$ is the entropy difference between the gas phase and adsorbed state. The entropies of free gases were acquired from the NIST database.

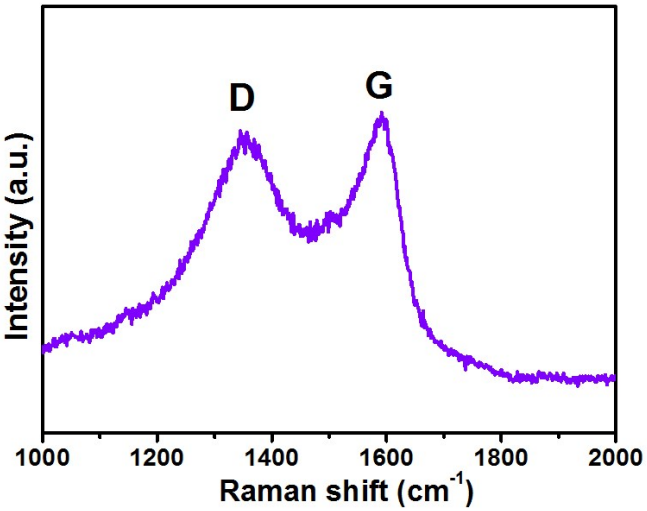

Fig. S1. Raman spectra of $MnMoO_4$/RGO.

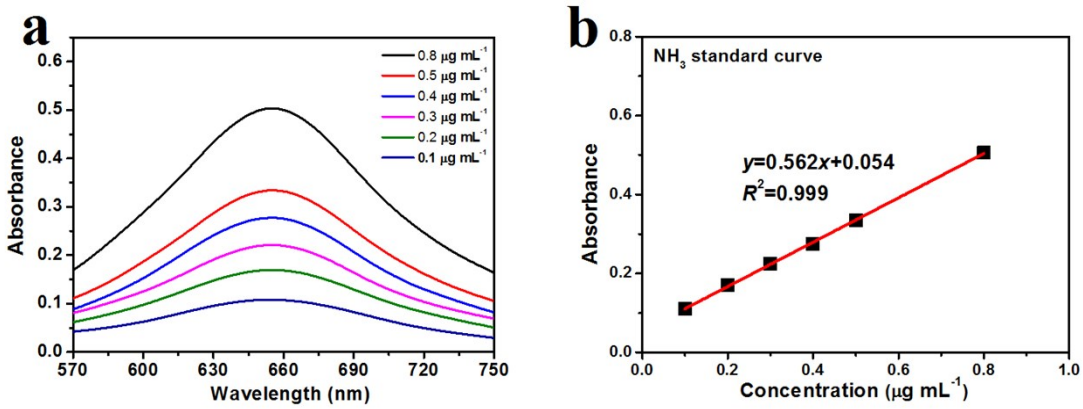

Fig. S2. (a) UV-Vis absorption spectra of indophenol assays with NH_4Cl after incubated for 2 h at ambient conditions. (b) Calibration curve used for calculation of NH_3 concentrations.

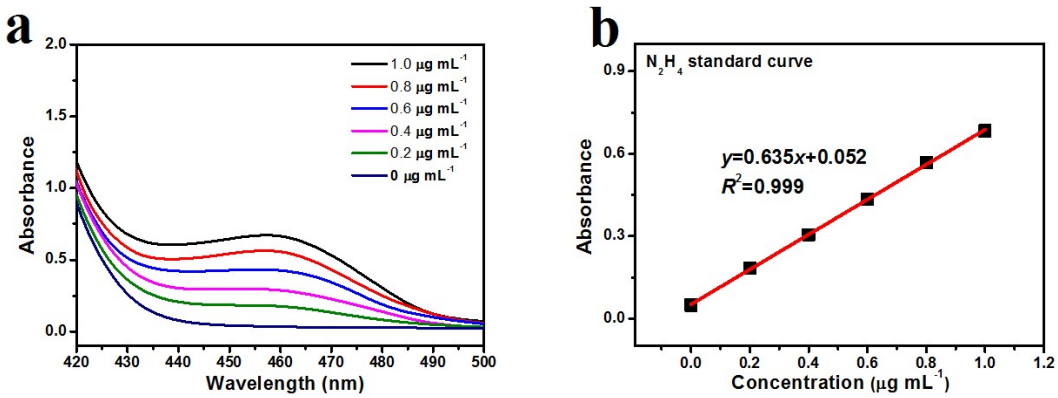

Fig. S3. (a) UV-Vis absorption spectra of N_2H_4 assays after incubated for 20 min at ambient conditions. (b) Calibration curve used for calculation of N_2H_4 concentrations.

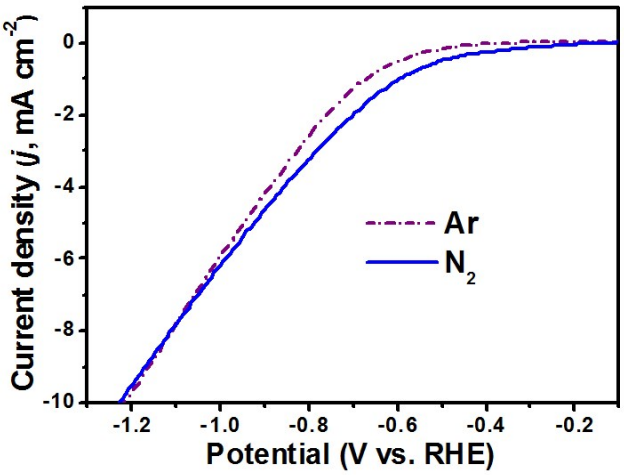

Fig. S4. LSV curves of $MnMoO_4$/RGO in Ar- and N_2- saturated solutions.

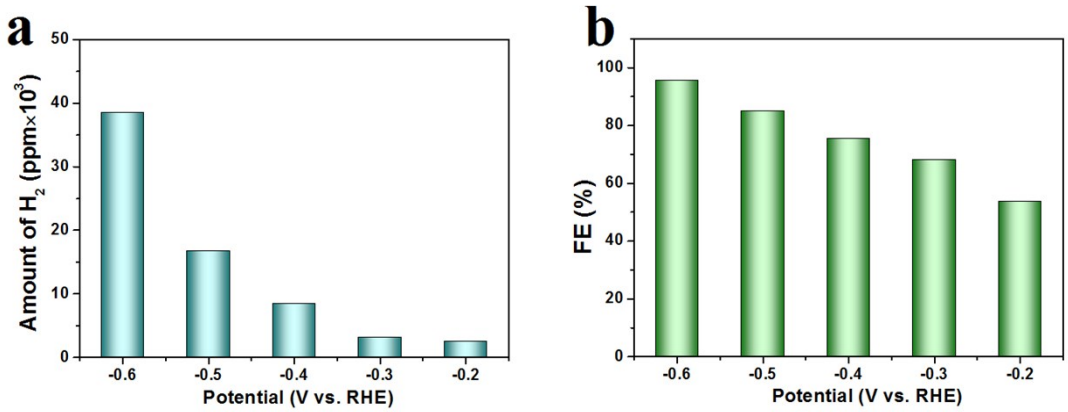

Fig. S5. (a) Amounts of produced H_2 and (b) corresponding FE of H_2 yield at various potentials.

The FE for H_2 yield can be calculated by [6]

$$\text{FE}\ (\%) = \frac{2 \times F \times n}{Q} \times 100\% \tag{4}$$

where Q is the quantity of applied electricity. F is the Faraday constant, n is the actually produced H_2 (mol) obtained by gas chromatography (GC) analysis[7]. Combing the data with the FE for NH_3 selectivity (Fig. 2c), the unaccounted values result presumably from the capacitance of the support, and the dynamic hydrogen adsorption on the catalyst, as well as the uncontrollable experimental error[8].

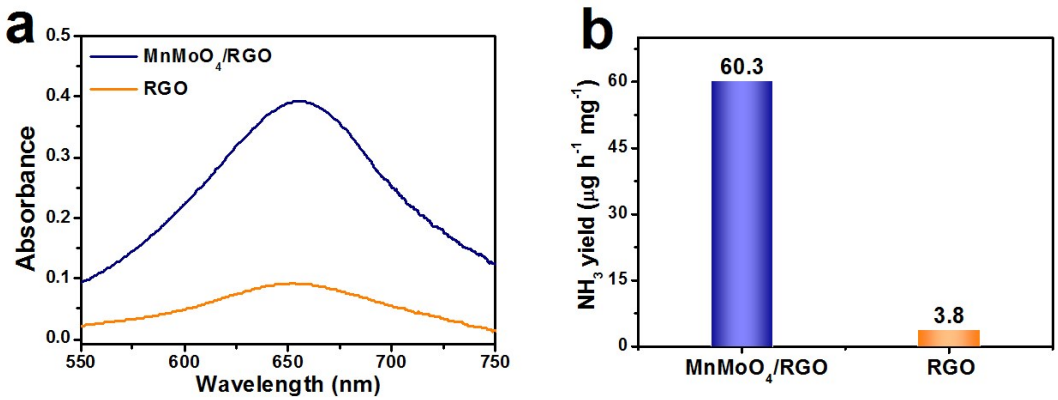

Fig. S6. (a) UV−vis absorption spectra of the electrolytes after 2 h of NRR electrolysis (-0.4 V) over $MnMoO_4$/RGO and RGO, and (b) corresponding NH_3 yields.

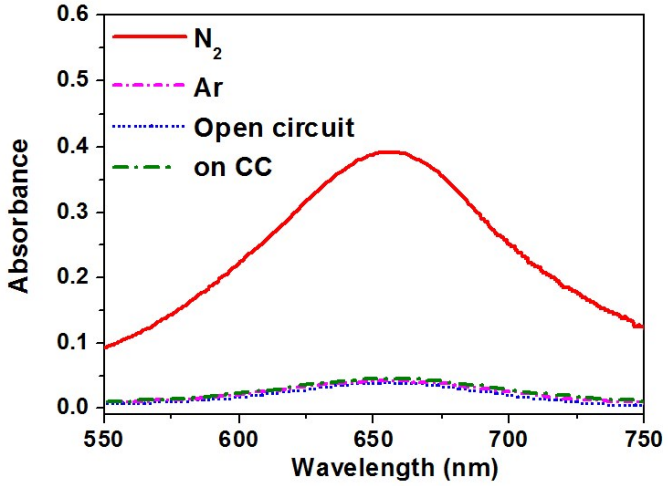

Fig. S7. UV-Vis absorption spectra of the electrolytes stained with indophenol indicator after 2 h electrolysis on $MnMoO_4$/RGO at -0.4 V in N_2-saturated solution, Ar-saturated solutions, N_2-saturated solution at open circuit and N_2-saturated solution on pristine CC.

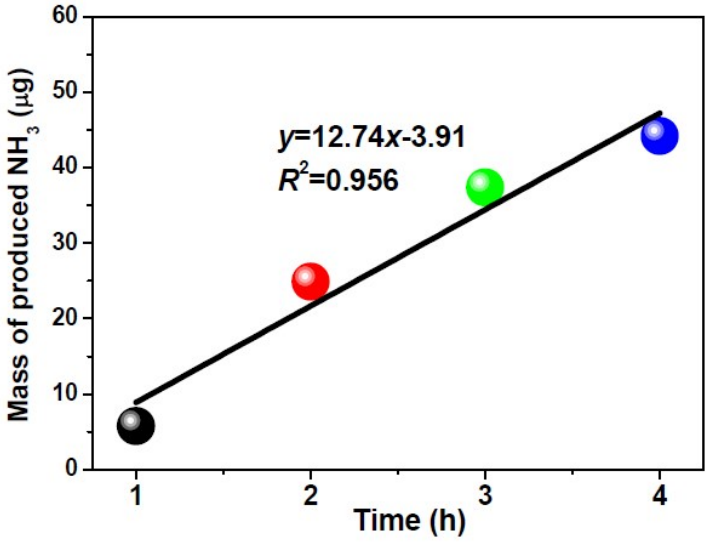

Fig. S8. Mass of produced NH_3 after NRR electrolysis at various times (1-4 h) on $MnMoO_4$/RGO at -0.4 V.

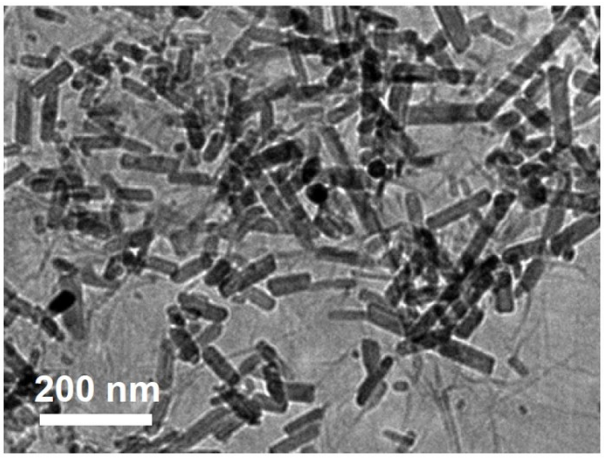

Fig. S9. TEM image of $MnMoO_4$/RGO after stability test.

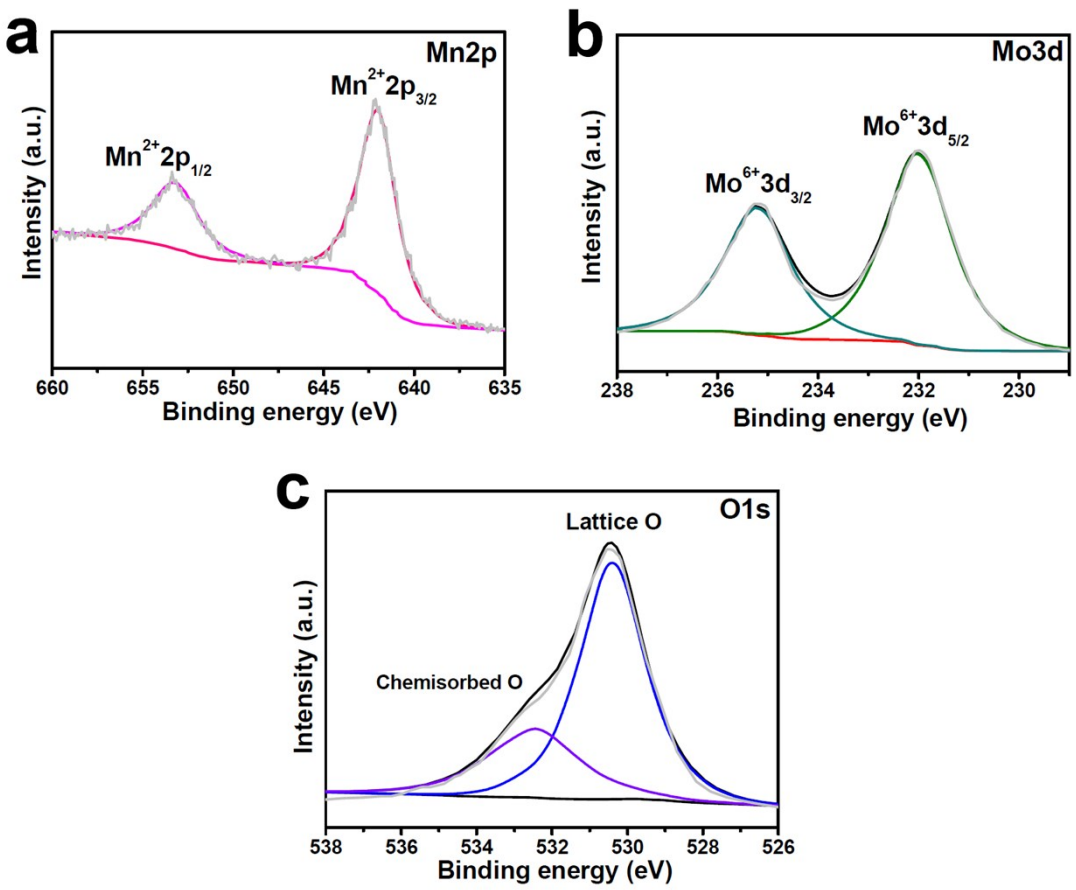

Fig. S10. XPS spectra of $MnMoO_4$/RGO after stability test: (a) Mn2p; (b) Mo3d; (c) O1s.

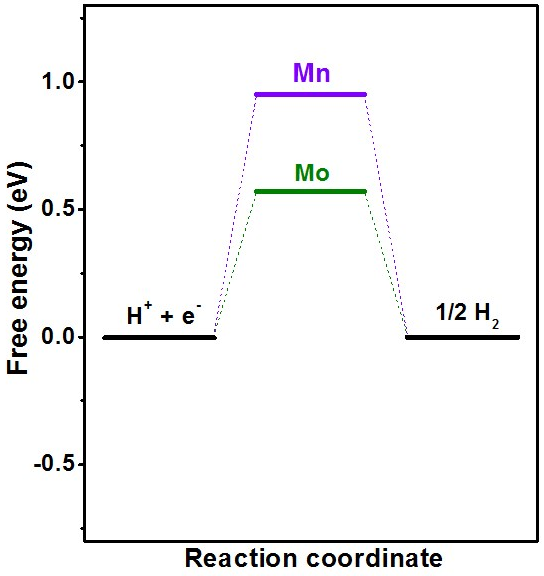

Fig. S11. Free energy diagrams of *H adsorption (G_{*H}) on Mn and Mo atoms of $MnMoO_4$ (220) facet.

Table S1. Comparison of optimum NH_3 yield and Faradic efficiency (FE) for recently reported state-of-the-art NRR electrocatalysts at ambient conditions

Catalyst	Electrolyte	Determination method	Optimum Potential (V Vs RHE)	NH_3 yield ($\mu g\ h^{-1}\ mg^{-1}$)	FE (%)	Ref.
$Bi_4V_2O_{11}$-CeO_2 nanofibers	0.1 M HCl	Indophenol blue method	-0.2	23.21	10.16	[6]
CoP hollow nanocages	1.0 M KOH	Indophenol blue method	-0.4	10.78	7.36	[7]
S-doped carbon nanospheres	0.1 M Na_2SO_4	Indophenol blue method	-0.7	19.07	7.47	[8]
Fe_3S_4 nanosheets	0.1 M HCl	Indophenol blue method	-0.5	75.4	6.45	[9]
B_4C nanosheets	0.1 M HCl	Indophenol blue method	-0.75	26.57	15.95	[10]
Defect-rich MoS_2 nanoflower	0.1 M Na_2SO_4	Indophenol blue method	-0.4	29.28	8.34	[11]
MoS_2 with Li-S Interactions	0.1 M Li_2SO_4	Indophenol blue method	-0.2	43.4	9.81	[12]
Mo_2C/C	0.5 M Li_2SO_4	Nessler's reagent method	-0.3	11.3	7.8	[13]
MoO_2 with oxygen vacancies	0.1 M HCl	Indophenol blue method	-0.15	12.2	8.2	[14]
Mo single atoms	0.1 M KOH	Indophenol blue method	-0.3	34	14.6	[15]
MoO_3 nanosheets	0.1 M HCl	Indophenol blue method	-0.5	29.43	1.9	[16]
MoO_2/graphene	0.1 M Na_2SO_4	Indophenol blue method	-0.35	37.4	6.6	[17]
MnO particles	0.1 M Na_2SO_4	Indophenol blue method	-0.39	7.92	8.02	[18]
Mn_3O_4 nanocubes	0.1 M Na_2SO_4	Indophenol blue method	-0.8	11.6	3	[19]
Mn_3O_4/RGO	0.1 M Na_2SO_4	Indophenol blue method	-0.85	17.4	3.52	[20]
MnO_2-$Ti_3C_2T_x$ MXene nanohybrid	0.1 M HCl	Indophenol blue method	-0.55	34.12	11.39	[21]
$MnMoO_4$/RGO	**0.5 M $LiClO_4$**	**Indophenol blue method**	**-0.4**	**60.3**	**14.7 (-0.3 V)**	**This work**

Supplementary references

[1]. B. Hu, M. Hu, L. C. Seefeldt and T. L. Liu, *ACS Energy Lett.*, 2019, **4**, 1053-1054.

[2]. D. Zhu, L. Zhang, R. E. Ruther and R. J. Hamers, *Nat. Mater.*, 2013, **12**, 836.

[3]. G. W. Watt and J. D. Chrisp, *Anal. Chem.*, 1952, **24**, 2006-2008.

[4]. S. J. Clark, M. D. Segall, C. J. Pickard, P. J. Hasnip, M. I. J. Probert, K. Refson and M. C. Payne, *Z. Kristallogr.*, 2005, **220**, 567-570.

[5]. A. A. Peterson, *Energy Environ. Sci.*, 2010, **3**, 1311-1315.

[6]. C. Lv, C. Yan, G. Chen, Y. Ding, J. Sun, Y. Zhou and G. Yu, *Angew. Chem. Int. Edit.*, 2018, **130**, 6181-6184.

[7]. W. Guo, Z. Liang, J. Zhao, B. Zhu, K. Cai, R. Zou and Q. Xu, *Small Methods*, 2018, **2**, 1800204.

[8]. L. Xia, X. Wu, Y. Wang, Z. Niu, Q. Liu, T. Li, X. Shi, A. M. Asiri and X. Sun, *Small Methods*, 2018, **3**, 1800251.

[9]. X. Yu, P. Han, Z. Wei, L. Huang, Z. Gu, S. Peng, J. Ma and G. Zheng, *Joule*, 2018, **2**, 1610-1622.

[10]. W. Qiu, X.-Y. Xie, J. Qiu, W.-H. Fang, R. Liang, X. Ren, X. Ji, G. Cui, A. M. Asiri and G. Cui, *Nat. Commun.*, 2018, **9**, 3485.

[11]. X. Li, T. Li, Y. Ma, Q. Wei, W. Qiu, H. Guo, X. Shi, P. Zhang, A. M. Asiri and L. Chen, *Adv. Energy. Mater.*, 2018, **8**, 1801357.

[12]. Y. Liu, M. Han, Q. Xiong, S. Zhang, C. Zhao, W. Gong, G. Wang, H. Zhang and H. Zhao, *Adv. Energy. Mater.*, 2019, **9**, 1803935.

[13]. H. Cheng, L. X. Ding, G. F. Chen, L. Zhang, J. Xue and H. Wang, *Adv. Mater.*, 2018, **30**, 1803694.

[14]. G. Zhang, Q. Ji, K. Zhang, Y. Chen, Z. Li, H. Liu, J. Li and J. Qu, *Nano Energy*, 2019, **59**, 10-16.

[15]. L. Han, X. Liu, J. Chen, R. Lin, H. Liu, F. Lu, S. Bak, Z. Liang, S. Zhao and E. Stavitski, *Angew. Chem. Int. Edit.*, 2018, **58**, 2321-2325.

[16]. J. Han, X. Ji, X. Ren, G. Cui, L. Li, F. Xie, H. Wang, B. Li and X. Sun, *J. Mater. Chem. A*, 2018, **6**, 12974-12977.

[17]. J. Wang, Y. P. Liu, H. Zhang, D. J. Huang and K. Chu, *Catal. Sci. Technol.*, 2019, **9**, 4248-4254.

[18]. Z. Wang, F. Gong, L. Zhang, R. Wang, L. Ji, Q. Liu, Y. Luo, H. Guo, Y. Li, P. Gao, X. Shi, B. Li, B. Tang and X. Sun, *Adv. Sci.*, 2018, 1801182.

[19]. X. Wu, L. Xia, Y. Wang, W. Lu, Q. Liu, X. Shi and X. Sun, *Small*, 2018, **14**, 1803111.

[20]. H. Huang, F. Gong, Y. Wang, H. Wang, X. Wu, W. Lu, R. Zhao, H. Chen, X. Shi, A. M. Asiri, T. Li, Q. Liu and X. Sun, *Nano Res.*, 2019, **12**, 1093-1098.

[21]. W. Kong, F. Gong, Q. Zhou, G. Yu, L. Ji, X. Sun, A. M. Asiri, T. Wang, Y. Luo and Y. Xu, *J. Mater. Chem. A*, 2019, **7**, 18823-18827.